Preparation and Luminescence Properties of YVO_4:Ln and Y(V, P)O_4:Ln (Ln = Eu^{3+}, Sm^{3+}, Dy^{3+}) Nanofibers and Microbelts by Sol−Gel/Electrospinning Process

Zhiyao Hou,[†,‡] Piaoping Yang,[†,‡] Chunxia Li,[†] Lili Wang,[†] Hongzhou Lian,[†] Zewei Quan,[†] and Jun Lin*[,†]

State Key Laboratory of Rare Earth Resource Utilization, Changchun Institute of Applied Chemistry, Chinese Academy of Sciences, Changchun 130022, People's Republic of China, and College of Materials Science and Chemical Engineering, Harbin Engineering University, Harbin 150001, People's Republic of China

Received June 6, 2008. Revised Manuscript Received August 22, 2008

One-dimensional YVO_4:Ln and Y(V, P)O_4:Ln nanofibers and quasi-one-dimensional YVO_4:Ln microbelts (Ln = Eu^{3+}, Sm^{3+}, Dy^{3+}) have been prepared by a combination method of sol−gel process and electrospinning. X-ray diffraction (XRD), Fourier transform infrared spectroscopy (FT-IR), thermogravimetric and differential thermal analysis (TG−DTA), scanning electron microscopy (SEM), transmission electron microscopy (TEM), high-resolution transmission electron microscopy (HRTEM), photoluminescence (PL), low-voltage cathodoluminescence (CL), and time-resolved emission spectra as well as kinetic decays were used to characterize the resulting samples. Due to an efficient energy transfer from vanadate groups to dopants, YVO_4:Ln phosphors showed their strong characteristic emission under ultraviolet excitation (280 nm) and low-voltage electron beam excitation (1−3 kV). The energy transfer process was further studied by the time-resolved emission spectra as well as kinetic decay curves of Eu^{3+} upon excitation into the VO_4^{3-} ion. Furthermore, the PL emission color of YVO_4:Ln nanofibers can be tuned from blue to green, orange-red, and red easily by partial replacement VO_4^{3-} with PO_4^{3-} and changing the doping concentrations (x) of Ln, making the materials have potential applications in fluorescent lamps and field emission displays (FEDs).

1. Introduction

One-dimensional (1D) nanomaterials including nanowires, nanofibers, nanotubes, and nanorods have attracted great research interest[1−4] because of their specific and fascinating properties, such as high luminescence efficiency, superior mechanical toughness, metal insulator transition, and lowered threshold.[5] Quasi-one-dimensional (Q-1D) nanostructures also have attracted intensive experimental and theoretical interest as a result of their novel physical properties and potential application.[6] As one subgroup of Q-1D nanostructures, nanobelts not only help to extend the understanding of the relationships between structure and property but can also contribute to an ideal system for building functional devices. Exploring nanobelts with very large widths on the micrometer, microbelts still remain significant on promising properties.[7] 1D and Q-1D nanomaterials with different compositions have been developed using various methods including chemical or physical vapor deposition,[8] laser ablation,[9] solution,[5b,10] arc discharge,[11] vapor-phase transport process,[12] and a template-based method.[13] In comparison to these, electrospinning is an effective and simple method for preparing nanofibers from a rich variety of materials,[14] such

* Corresponding author. E-mail: jlin@ciac.jl.cn.
† Changchun Institute of Applied Chemistry.
‡ Harbin Engineering University.

(1) Xia, Y.; Yang, P.; Sun, Y.; Wu, Y.; Gates, B.; Yin, Y.; Kim, F.; Yan, H. *Adv. Mater.* **2003**, *15*, 353.
(2) Bockrath, M.; Liang, W.; Bozovic, D.; Hafner, J. H.; Lieber, C. M.; Tinkham, M.; Park, H. *Science* **2001**, *291*, 283.
(3) Huang, Y.; Quan, X. F.; Wei, Q. Q.; Lieber, C. M. *Science* **2001**, *291*, 851.
(4) Li, D.; Xia, Y. *Nano Lett.* **2003**, *3*, 555.
(5) (a) Wang, E. W.; Sheehan, P. E.; Lieber, C. M. *Science* **1997**, *277*, 1971. (b) Holmes, J. D.; Johnston, K. P.; Doty, R. C.; Korgel, B. A. *Science* **2000**, *287*, 1471. (c) Hicks, L. D.; Dresselhaus, M. S. *Phys. Rev. B* **1996**, *47*, 16631. (d) Miyamoto, Y.; Miyake, Y.; Asada, M.; Suematsu, Y. *J. Quantum Electron.* **1989**, *25*, 2001. (e) Arakawa, Y.; Sakaki, H. *Appl. Phys. Lett.* **1982**, *40*, 939.
(6) (a) Alivisator, A. P. *Science* **1996**, *271*, 933. (b) Wong, E. W.; Sheehan, P. E.; Lieber, C. M. *Science* **1997**, *277*, 1971. (c) Hu, J.; Odom, T. W.; Lieber, C. M. *Acc. Chem. Res.* **1999**, *32*, 435.
(7) (a) Shen, G. Z.; Cho, J. H.; Yoo, J. K.; Yi, G. C.; Lee, C. J. *J. Phys. Chem. B* **2005**, *109*, 9294. (b) Zhang, J.; Jiang, F. H.; Yang, Y. D.; Li, J. P. *J. Phys. Chem. B* **2005**, *109*, 13143. (c) Zhao, Y.; Zhu, X.; Huang, Y. Y.; Wang, S. X.; Yang, J. L.; Xie, Y. *J. Phys. Chem. C* **2007**, *111*, 12145.
(8) (a) Yazawa, M.; Koguchi, M.; Muto, A.; Ozawa, M.; Hiruma, K. *Appl. Phys. Lett.* **1992**, *61*, 2051. (b) Bae, S. Y.; Seo, H. W.; Park, J.; Yang, H.; Park, J. C.; Lee, S. Y. *Appl. Phys. Lett.* **2002**, *81*, 126. (c) Fu, L.; Liu, Y. Q.; Hu, P.; Xiao, K.; Yu, G.; Zhu, D. B. *Chem. Mater.* **2003**, *15*, 4287. (d) Yu, J. G.; Yu, J. C.; Ho, W. K.; Wu, L.; Wang, X. C. *J. Am. Chem. Soc.* **2004**, *126*, 3422.
(9) (a) Duan, X. F.; Lieber, C. M. *Adv. Mater.* **2000**, *12*, 298. (b) Yazawa, M.; Koguchi, M.; Muto, A.; Ozawa, M.; Hiruma, K. *Appl. Phys. Lett.* **1992**, *61*, 2051.
(10) Trentler, T. J.; Hickman, K. M.; Goel, S. C.; Viano, A. M.; Gibbons, P. C.; Buhro, W. E. *Science* **1995**, *270*, 1791.
(11) (a) Choi, Y. C.; Kim, W. S.; Park, Y. S.; Lee, S. M.; Bae, D. J.; Lee, Y. H.; Park, G. S.; Choi, W, B.; Lee, N. S.; Kim, J. M. *Adv. Mater.* **2000**, *12*, 746. (b) Jung, J. H.; Kobayashi, H.; Van Bommel, K. J. L.; Shinkai, S.; Shimizu, T. *Chem. Mater.* **2002**, *14*, 1445.
(12) (a) Wu, Y.; Yang, P. *Chem. Mater.* **2000**, *12*, 605. (b) Chen, C. C.; Yeh, C. C. *Adv. Mater.* **2000**, *12*, 738. (c) Bai, Z. G.; Yu, D. P.; Zhang, H. Z.; Ding, Y.; Gai, X. Z.; Hang, Q. L.; Xiong, G. C.; Feng, S. Q. *Chem. Phys. Lett.* **1999**, *303*, 311.

10.1021/cm801538t CCC: $40.75
Published on Web 10/16/2008

as polymers and inorganic and hybrid (organic−inorganic) compounds.

The electrospinning technique has been developed since 1934 for the synthesis of 1D nanomaterials.[15] It is a process which uses the strong electrostatic force by a high static voltage applied to a polymer solution placed into a container with a millimeter diameter nozzle. Under applied electrical force, the polymer solution is ejected from the nozzle. After the solvents are evaporated during the course of jet spraying, the nanofibers are collected on a grounded collector. On the other hand, the sol−gel process has been proved as an efficient way to produce nanoparticles[16] and nanocoatings[17] of metal oxide. Sol−gel techniques can be employed to prepare precursor solutions, which have been used to deposit coatings by spinning and dipping processes.[18] In the past few years, our group has extended the application of the sol−gel process combining with other methods to fabricate various kinds of optical materials, mainly luminescence and pigment materials with different forms (powder, core−shell structures, thin film, and patterning).[19] 1D nanomaterials fabricated by a combination method of sol−gel process and electrospinning have become important for their exceptionally long length, uniform diameter, diverse composition, and high surface, which can be applied in biomedical fields, reinforced composites, catalyst supports, sensors, electronic and optical devices, as well as sacrificial templates.[20]

Among all the nanomaterials, rare earth compounds have been widely used in the fields of high-performance luminescent devices, catalysts, and other functional materials based on their electronic, optical, and chemical characteristics arising from their 4f electrons.[21] Furthermore, the rare earth compounds fabricated in the form of 1D or Q-1D nanostructure are expected to be highly functionalized materials as a result of both shape-specific and quantum confinement effects, acting as electrically, magnetically, and optically functional host materials as well. In comparison with bulk materials, the shape of a 1D structure provided a better model system to investigate the dependence of electronic transport and optical properties on size confinement and dimensionality.

Yttrium vanadate (YVO_4) has been shown to be a useful host lattice for rare earth ions to produce phosphors emitting a variety of colors, since high luminescence quantum yields are observed for the f−f transitions.[22] The previous work mainly focused on the Eu^{3+}-doped YVO_4 with different synthetic methods,[23] because it was an important commercial red-emitting phosphor used in color television, the high-pressure mercury lamp, and as a scintillator in medical image detectors.[24] Besides europium ion, Dy^{3+} and Sm^{3+} ions can also act as useful activators. Dy^{3+}-doped YVO_4 is a potential white phosphor because of the yellow ($^4F_{9/2}-{}^6H_{13/2}$) and blue ($^4F_{9/2}-{}^6H_{15/2}$) emissions of Dy^{3+}, and Sm^{3+}-doped YVO_4 yields characteristic red-orange emission of Sm^{3+} at 567 ($^4G_{5/2}-{}^6H_{5/2}$), 605 ($^4G_{5/2}-{}^6H_{7/2}$), and 649 ($^4G_{5/2}-{}^6H_{9/2}$) nm. In addition, by partial replacement of $VO_4{}^{3-}$ ions with $PO_4{}^{3-}$ ions, a new series of Ln-doped yttrium phosphate–vanadates ($YV_{1-x}P_xO_4$) have emerged with better luminescent properties.[25] Although the investigations on YVO_4:Ln and $YV_{1-x}P_xO_4$:Ln phosphors are extensive, little study has been reported on synthesis of 1D or Q-1D YVO_4:Ln and Y(V, P)O_4:Ln together with their luminescent properties by electrospinning process. Accordingly, in this paper, we report the preparation of Q-1D beltlike YVO_4:Ln and 1D fiberlike YVO_4:Ln and $YP_{0.8}V_{0.2}O_4$:Ln (Ln = Eu^{3+}, Sm^{3+}, Dy^{3+}) phosphors through a combination method of sol−gel process and electrospinning, as well as their photoluminescent and cathodoluminescent properties.

(13) (a) Huang, M. H.; Choudrey, A.; Yang, P. *Chem. Commun.* **2000**, *12*, 1603. (b) Zhu, J.; Fan, S. *J. Mater. Res.* **1999**, *14*, 1175. (c) Li, Y.; Meng, G. W.; Zhang, L. D.; Phillipp, F. *Appl. Phys. Lett.* **2000**, *76*, 2011.

(14) (a) Madhugiri, S.; Dalton, A.; Gutierrez, J.; Ferraris, J. P.; Balkus, K. J., Jr. *J. Am. Chem. Soc.* **2003**, *125*, 14531. (b) Yao, L.; Haas, T. W.; Guiseppi-Elie, A.; Bowlin, G. L.; Simpson, D. G.; Wnek, G. E. *Chem. Mater.* **2003**, *15*, 1860. (c) Larsen, G.; Velarde-Ortiz, R.; Minchow, K.; Barrero, A.; Loscertales, I. G. *J. Am. Chem. Soc.* **2003**, *125*, 1154. (d) Hou, H. Q.; Reneker, D. H. *Adv. Mater.* **2004**, *16*, 69. (e) Wu, J.; Coffer, J. L. *Chem. Mater.* **2007**, *19*, 6266. (f) Ge, J. J.; Hou, H.; Li, Q.; Graham, M. J.; Greiner, A.; Reneker, D. H.; Harris, F. W.; Cheng, S. Z. D. *J. Am. Chem. Soc.* **2004**, *126*, 15754. (g) Li, M. J.; Zhang, J. H.; Zhang, H.; Liu, Y. F.; Wang, C. L.; Xu, X.; Tang, Y.; Yang, B. *Adv. Funct. Mater.* **2007**, *17*, 3650.

(15) Formhals, A. *U.S. Pat. Specif.* **1934**, *1*, 975–504.

(16) Yang, P.; Lu, M. K.; Song, C. F.; Zhou, G. J.; Xu, D.; Yuan, D. R. *J. Phys. Chem. Solids* **2002**, *63*, 2047.

(17) Fu, X. A.; Qutubuddin, S. *Colloid Surf., A* **2001**, *186*, 245.

(18) Zhai, J. W.; Zhang, L. Y.; Yao, X.; Hodgson, S. N. B. *Surf. Coat. Technol.* **2001**, *138*, 135.

(19) (a) Liu, X. M.; Lin, C. K.; Luo, Y.; Lin, J. *J. Electrochem. Soc.* **2007**, *154*, 121. (b) Liu, X. M.; Lin, J. *J. Appl. Phys.* **2006**, *100*, 124306. (c) Yu, M.; Lin, J.; Fang, J. *Chem. Mater.* **2005**, *17*, 1783. (d) Lin, C. K.; Li, Y. Y.; Yu, M.; Yang, P. P.; Lin, J. *Adv. Funct. Mater.* **2007**, *17*, 1459. (e) Yu, M.; Lin, J.; Wang, Z.; Fu, J.; Wang, S.; Zhang, H. J.; Han, Y. C. *Chem. Mater.* **2002**, *14*, 2224.

(20) (a) Bergshoef, M. M.; Vancso, G. J. *Adv. Mater.* **1999**, *11*, 1362. (b) Wang, X. Y.; Drew, C.; Lee, S. H.; Senecal, K. J.; Kumar, J.; Samuelson, L. A. *Nano Lett.* **2002**, *2*, 1273. (c) Liu, H. Q.; Kameoka, J.; Czaplewski, D. A.; Craighead, H. G. *Nano Lett.* **2004**, *4*, 671. (d) Casper, C. L.; Stephens, J. S.; Tassi, N. G.; Chase, D. B.; Rabolt, J. F. *Macromolecules* **2004**, *37*, 573. (e) Hou, H. Q.; Jun, Z.; Reuning, A.; Schaper, A.; Wendorff, J. H.; Greiner, A. *Macromolecules* **2002**, *35*, 2429. (f) Czaplewski, D. A.; Verbridge, S. S.; Kameoka, J.; Craighead, H. G. *Nano Lett.* **2004**, *4*, 437. (g) Czaplewski, D. A.; Kameoka, J.; Mathers, R.; Coates, G. W.; Craighead, H. G. *Appl. Phys. Lett.* **2003**, *83*, 4836. (h) Yu, H. Q.; Song, H. W.; Pan, G. H.; Qin, R. F.; Fan, L. B.; Zhang, H.; Bai, X.; Li, S. W.; Zhao, H. F.; Lu, S. Z. *J. Nanosci. Nanotechnol.* **2008**, *8*, 1432.

(21) (a) Tang, Q.; Liu, Z. P.; Li, S.; Zhang, S. Y.; Liu, X. M.; Qian, Y. T. *J. Cryst. Growth* **2003**, *259*, 208. (b) Capobianco, J. A.; Vetrone, F.; Boyer, J. C.; Speghini, A.; Bettinelli, M. *Opt. Mater.* **2002**, *19*, 259. (c) Palmer, M. S.; Neurock, M.; Olken, M. M. *J. Am. Chem. Soc.* **2002**, *124*, 8452. (d) Hasegawa, Y.; Thongchant, S.; Wada, Y.; Tanaka, H.; Kawai, T.; Sakata, T.; Mori, H.; Yanagida, S. *Angew. Chem.* **2002**, *114*, 2177.

(22) (a) Riwotzki, K.; Haase, M. *J. Phys. Chem. B* **1998**, *102*, 10129. (b) Huignard, A.; Gacoin, T.; Boilot, J. P. *Chem. Mater.* **2000**, *12*, 1090. (c) Hsu, C.; Powell, R. C. *J. Lumin.* **1975**, *10*, 273. (d) Wu, X. C.; Tao, Y. R.; Song, C. Y.; Mao, C. J.; Dong, L.; Zhu, J. J. *J. Phys. Chem. B* **2006**, *110*, 15791.

(23) (a) Haase, M.; Riwotzki, K.; Meyssamy, H.; Kornowski, A. *J. Alloys Compd.* **2000**, *303*, 191. (b) Huignard, A.; Buissette, V.; Laurent, G.; Gacoin, T.; Boilot, J. P. *Chem. Mater.* **2002**, *14*, 2264. (c) Yan, C. H.; Sun, L. D.; Liao, C. S. *Appl. Phys. Lett.* **2003**, *82*, 3511.

(24) (a) Schwarz, H. *Z. Anorg. Allg. Chem.* **1963**, *323*, 44. (b) Wanmaker, W. L.; Bril, A.; Vrugt, J. W.; Broos, J. *Philips Res. Rep.* **1966**, *21*, 270. (c) Brecher, C.; Samelson, H.; Lempicki, A.; Riley, R.; Peters, T. *Phys. Rev.* **1967**, *155*, 178 (6)–835. (d) Venikouas, G. E.; Powell, R. C. *J. Lumin.* **1978**, *16*, 29. (e) Riwotzki, K.; Haase, M. *J. Phys. Chem. B* **2001**, *105*, 12709.

(25) (a) Yu, M.; Lin, J.; Wang, S. B. *Appl. Phys. A: Mater. Sci. Process.* **2005**, *80*, 353. (b) Wang, F.; Xue, X. J.; Liu, X. G. *Angew. Chem., Int. Ed.* **2008**, *47*, 804. (c) Wu, C. C.; Chen, K. B.; Lee, C. S.; Chen, T. M.; Cheng, B. M. *Chem. Mater.* **2007**, *19*, 3278.

2. Experimental Section

2.1. Preparation. Nanofibers of YVO_4:Ln (Ln = Eu^{3+}, Sm^{3+}, Dy^{3+}) phosphors were prepared by a method of sol−gel process and electrospinning. The stoichiometric amounts of Y_2O_3, Eu_2O_3, Sm_2O_3, Dy_2O_3 (all with purity of 99.999%, Science and Technology Parent Company of Changchun Institute of Applied Chemistry, China) and NH_4VO_3 (99%, analytical reagent, AR) were dissolved in dilute nitric acid HNO_3 (AR) and then were mixed with a water−ethanol (v/v = 1:4) solution containing citric acid (AR) as a chelating agent for the metal ions. The molar ratio of metal ions to citric acid was 1:2. A certain amount of poly(vinylpyrrolidone) (PVP, M_w = 1 300 000, Aldrich) was added to adjust the viscoelastic behavior of the solution (the weight percentage of PVP is 7% in the water−ethanol solution). The solution was stirred for 4 h to obtain a homogeneous hybrid sol for further electrospinning. The distance between the spinneret (a metallic needle) and collector (a grounded conductor) was fixed at 17 cm, and the high-voltage supply was maintained at 20 kV. The spinning rate was controlled at 0.5 mL·h^{-1} by a syringe pump (TJ-3A/W0109-1B, Boading Longer Precision Pump Co., Ltd., China). The as-prepared hybrid precursor samples were annealed to the desired temperature (400−900 °C) with the heating rate of 2 °C·min^{-1} and held there for 4 h in air. Through partial replacement of NH_4VO_3 with $(NH_4)H_2PO_4$ (AR), $YP_{0.8}V_{0.2}O_4$:Ln nanofibers were obtained under the same experimental conditions as those for the preparation of YVO_4:Ln nanofibers. In a typical process for the preparation of YVO_4:Ln microbelts, the solution for electrospinning was prepared by the similar procedure via changing the ratio of water−ethanol solution together with the type and amount of PVP. Typically, the ratio of water−ethanol solution was adjusted to 2:3 in volume, another kind of poly(vinylpyrrolidone) (PVP, K-30, Sinopharm Chemical Reagent Co., Ltd.) was added with a weight percentage of 25% in the water−ethanol solution. The solution was also stirred for 4 h to obtain a homogeneous hybrid sol for electrospinning. The distance between the spinneret and collector was tuned to 15 cm, and the high-voltage supply was changed to 30 kV. The spinning rate was controlled at 1 mL·h^{-1} by a syringe pump. The as-formed hybrid precursor samples were annealed to the desired temperature with the heating rate of 2 °C·min^{-1} and maintained for 4 h in air. In this way, YVO_4:Ln and $YP_{0.8}V_{0.2}O_4$:Ln nanofibers and YVO_4:Ln microbelts (Ln = Eu^{3+}, Sm^{3+}, Dy^{3+}) have been prepared. The detailed sample synthesis parameters and compositions (including the doping concentrations in synthesis and actual concentrations determined by analysis) are summarized in Tables S1 and S2 (Supporting Information), respectively.

2.2. Characterization. The X-ray diffraction (XRD) patterns of the samples were carried out on a Rigaku-Dmax 2500 diffractometer using Cu Kα radiation (λ = 0.15405 nm). Fourier transform infrared spectroscopy (FT-IR) spectra were performed on Perkin-Elmer 580B infrared spectrophotometer using the KBr pellet technique. Thermogravimetric and differential thermal analysis (TG−DTA) data were recorded with a Thermal Analysis instrument (SDT 2960, TA Instruments, New Castle, DE) with the heating rate of 10 °C·min^{-1} in an air flow of 100 mL·min^{-1}. The morphology of the samples was inspected using a field emission scanning electron microscope (SEM, Philips XL 30). Transmission electron microscopy (TEM) and high-resolution transmission electron microscopy (HRTEM) micrographs were obtained from an FEI Tecnai G2 S-Twin transmission electron microscope with a field emission gun operating at 200 kV. An inductively coupled plasma optical emission spectrometer (ICP-OES, ICAP 6300, Thermal Scientific) was used to determine the actual doping molar concentrations of Ln ions in YVO_4:Ln and Y(V, P)O_4:Ln samples and the actual V/P ratios in Y(V, P)O_4:Ln samples. The photoluminescence (PL) measurements were performed on a Hitachi F-4500 spectrophotometer equipped with a 150 W xenon lamp as the excitation source. The cathodoluminescence (CL) measurements were conducted in an ultrahigh-vacuum chamber ($<10^{-8}$ Torr), where the phosphors were excited by an electron beam at a voltage range of 1−3 kV with different filament currents 14−18 mA, and the emission spectra were recorded using an F-4500 spectrophotometer. The luminescence decay curves and time-resolved photoluminescence spectra were obtained from a Lecroy Wave Runner 6100 digital oscilloscope (1 GHz) using a tunable laser (pulse width = 4 ns, gate = 50 ns) as excitation (Continuum Sunlite OPO). All the measurements were performed at room temperature.

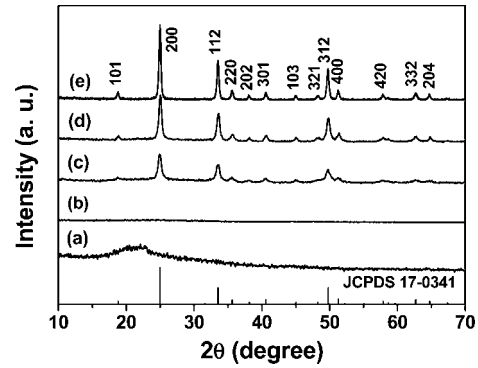

Figure 1. X-ray diffraction patterns for YVO_4:0.05Eu^{3+} nanofibers: (a) as-formed precursor fibers; the fibers annealed at (b) 400, (c) 500, (d) 700, and (e) 900 °C, respectively, as well as the JCPDS card 17-0341 of YVO_4 for comparison.

3. Results and Discussion

3.1. Formation and Morphology. *3.1.1. XRD.* Figure 1 shows the XRD patterns of the as-prepared precursor for YVO_4:0.05Eu^{3+} (fiberlike) sample and those annealed from 400 to 900 °C, as well as the JCPDS card (no. 17-0341) for YVO_4, respectively. In Figure 1a for the as-formed sample, no diffraction peak is observed except for the broad band at 2θ = 22°, which is ascribed to the semicrystalline PVP. When the precursor sample is calcined at 400 °C (Figure 1b), this broad peak disappears and no other diffraction peak is observed. This indicates the decomposition of PVP, and the sample still remains amorphous below this temperature. For the sample annealed at 500 °C (Figure 1c), well-defined diffraction peaks appear, all of which can be indexed to the tetragonal phase of YVO_4 according to the JCPDS card (no. 17-0341). This suggests the precursor sample has begun to crystallize into YVO_4 at this heating temperature. No additional peaks for other phases have been found, indicating that Eu^{3+} ions have been effectively built into the YVO_4 host lattice (note that a minor amount of $EuYO_4$ phase might form in this process, which cannot be detected by the XRD technique). After annealing at 700 (Figure 1d) and 900 (Figure 1e) °C, all the diffraction peaks increase in intensity due to the increase of crystallinity. The same situation holds for the YVO_4:0.05Eu^{3+} samples (beltlike) obtained under other experimental conditions and other compositions like $Y(P_{0.8}V_{0.2})O_4$:0.05Eu^{3+} (Figure S1, Supporting Information). It is known that, with the increase of the x value, the diffraction peaks of $Y(P_xV_{1-x})O_4$:Ln samples are gradually shifted away from the position of pure YVO_4 toward that of

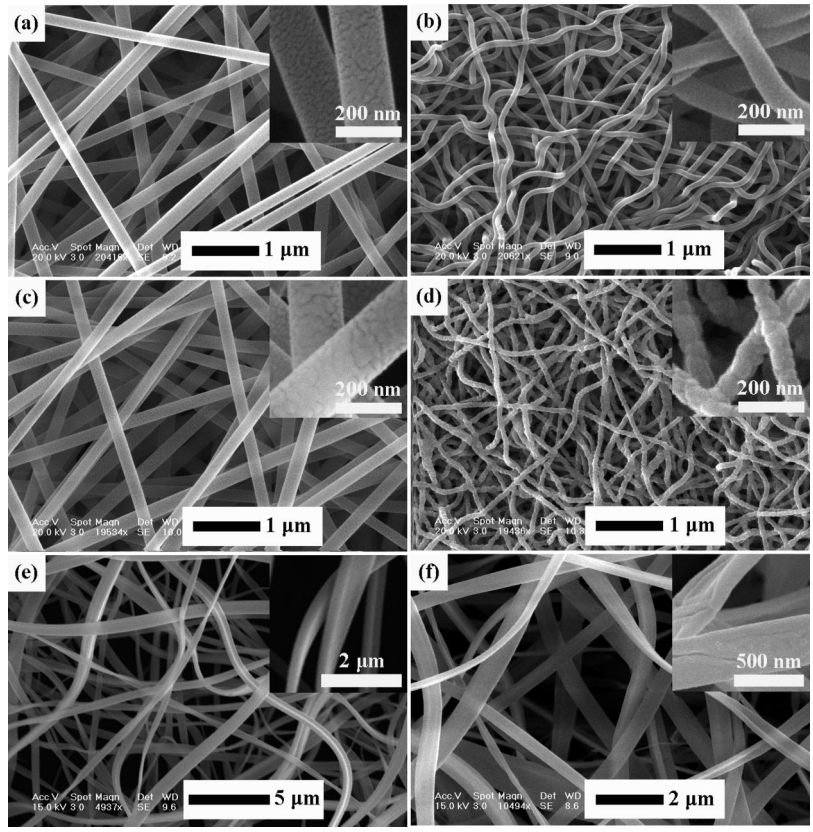

Figure 2. SEM images for the as-formed precursor for YVO_4:0.05Eu^{3+} nanofibers (a) and that annealed at 700 °C (b), the as-formed precursor for $YP_{0.8}V_{0.2}O_4$:0.05Eu^{3+} microfibers (c) and that annealed at 700 °C (d), the as-formed precursor for YVO_4:0.05Eu^{3+} microbelts (e) and that annealed at 700 °C (f).

YPO_4.[26] In Supporting Information Figure S1b, the diffraction peak at $2\theta = 25.5°$ for $x = 0.8$ is due to the (200) reflection of $Y(P_{0.8}V_{0.2})O_4$:0.05Eu^{3+}. The diffraction peaks of the $Y(P_{0.8}V_{0.2})O_4$:0.05Eu^{3+} (fiberlike) sample present 2θ values between the standard YVO_4 (JCPDS 17-0341) pattern and the standard YPO_4 (JCPDS 11-0254) pattern, agreeing well with the Vegard law. The diffraction peaks of YVO_4:Ln (Ln = Eu^{3+}, Sm^{3+}, Dy^{3+}) samples are shifted a little to lower angles with respect to the position of the standard YVO_4 (JCPDS 17-0341) pattern, as shown in Figure S2 (Supporting Information). This is because all the three Ln ions (Eu^{3+}, Sm^{3+}, Dy^{3+}) are bigger than Y^{3+} in the YVO_4 host lattice [for eight coordination, $R(Y^{3+}) = 0.1019$ nm, $R(Sm^{3+}) = 0.1079$ nm, $R(Eu^{3+}) = 0.1066$ nm, $R(Dy^{3+}) = 0.1027$ nm]. However, the shift is very small due to the low doping concentration of Ln^{3+}. Furthermore, the calculated crystal cell parameters ($a = 0.7122$ nm and $c = 0.6295$ nm) for the crystalline YVO_4:0.05Eu^{3+} nanofibers and those ($a = 0.7120$ nm and $c = 0.6292$ nm) for the YVO_4:0.05Eu^{3+} microbelts are slightly larger than the values ($a = 0.7118$ nm and $c = 0.6289$ nm) of pure YVO_4 (JCPDS 17-0341) due to the substitution of Y^{3+} by Eu^{3+}.

In general, the nanocrystallite size can be estimated from the Scherrer equation, $D = 0.89\lambda/\beta \cos\theta$, where D is the average grain size, λ is the X-ray wavelength (0.15405 nm), and θ and β are the diffraction angle and full width at half-maximum (in radian) of an observed peak, respectively.[27] The strongest peak (200) at $2\theta = 25°$ was used to calculate the average crystallite size (D) in the YVO_4:0.05Eu^{3+} nanofibers and microbelts. The estimated average crystallite sizes are 25 nm for the nanofibers and 30 nm for the microbelts, respectively.

3.1.2. FT-IR. The FT-IR spectra of the as-formed precursor YVO_4:0.05Eu^{3+} sample and those annealed from 500 to 900 °C are shown in Figure S3 (Supporting Information). In Supporting Information Figure S3a, for the as-formed precursor sample, the FT-IR spectrum shows the −OH group (3425 cm^{-1}), $-CH_2$ group (2957, 1475, and 1423 cm^{-1}), C═O group (1658 cm^{-1}), carbonates COO^- group (1384 cm^{-1}), and tertiary amine group (1291 cm^{-1}), which arise from the starting materials (ethanol, citric acid, and PVP).[19e,28] The absorption intensity of these bands decreases with the increase of annealing temperature because of the pyrolysis of the organic species. When the as-formed precursor sample was annealed at 500 °C (Supporting Information Figure S3b), a strong absorption band at 813 cm^{-1} and a weak band at 455 cm^{-1} have appeared, which can be attributed to the adsorption of V−O (from the VO_4^{3-} group) and Y−O bond, respectively.[19c,29] This indicated that yttrium vanadate

(26) Yu, M.; Lin, J.; Zhou, Y. H.; Pang, M. L.; Han, H. M.; Wang, S. B. *Thin Solid Films* **2003**, *444*, 245.

(27) (a) Zhang, Y. W.; Jin, S.; Tian, S. J.; Li, G. B.; Jia, T.; Liao, C. S.; Yan, C. H. *Chem. Mater.* **2001**, *13*, 372. (b) Nedelec, J. M.; Avignant, D.; Mahiou, R. *Chem. Mater.* **2002**, *14*, 651.

(28) (a) Lu, X. F.; Zhao, Y. Y.; Wang, C. *Adv. Mater.* **2005**, *17*, 2485. (b) Wu, J.; Coffer, J. L. *Chem. Mater.* **2007**, *19*, 6266. (c) Zhao, Y. Y.; Wang, H. Y.; Lu, X. F.; Li, X.; Yang, Y.; Wang, C. *Mater. Lett.* **2008**, *62*, 143.

(29) (a) Lin, J.; Sanger, D. V.; Menning, M.; Baerner, K. *Thin Solid Films* **2000**, *360*, 39. (b) Pang, M. L.; Lin, J.; Yu, M.; Wang, S. B. *J. Solid State Chem.* **2004**, *177*, 2236.

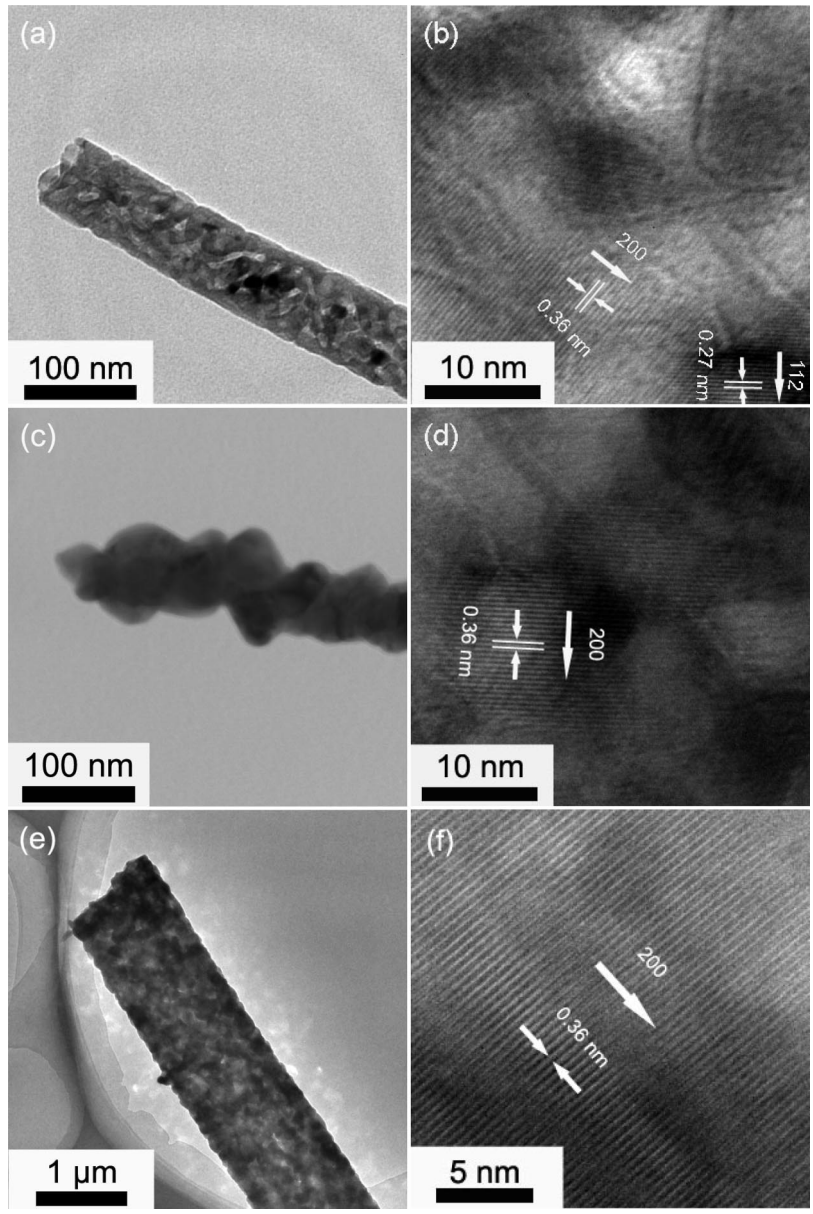

Figure 3. TEM images of YVO_4:0.05Eu^{3+} nanofibers (a) with its HRTEM (b), $YP_{0.8}V_{0.2}O_4$:0.05Eu^{3+} nanofibers (c) with its HRTEM (d), and YVO_4:0.05Eu^{3+} microbelts (e) with its HRTEM (f).

(YVO_4) began to become crystalline at 500 °C, agreeing well with the results of XRD. With the increase of the sintering temperature (Supporting Information Figure S3, parts c and d), the V−O bond becomes stronger and the absorption of organic impurities disappears, which is caused by the enhanced crystallinity with further annealing treatment.

3.1.3. TG−DTA. Figure S4 (Supporting Information) shows the TG−DTA curves of the as-formed precursor YVO_4:0.05Eu^{3+} sample heat-treated in air. The TG curve shows four stages of weight loss. The first weight loss (5%) step is observed between 40 and 90 °C due to the evaporation of water and organic solvents. The second weight loss (20%) from 90 to 260 °C accompanied by an exothermic peak at 103 °C in the DTA curve can be associated with the burnout of excess water, citric acid, and ethanol. The third weight loss step (50%) between 260 and 400 °C accompanied by a strong exothermic peaks at 285 °C in the DTA curve may be due to the further combustion of the organic groups in PVP, citric acid, and the citrates.[30] Finally, the weight loss (16%) is from 400 to 600 °C accompanied with an exothermic band between 430 and 520 °C in the DTA curve because of the crystallization of the YVO_4 phase, basically agreeing with the results of XRD and FT-IR.

3.1.4. SEM and TEM. Figure 2 shows the SEM micrographs of the as-formed precursors for YVO_4:0.05Eu^{3+} (fibers), $YP_{0.8}V_{0.2}O_4$:0.05Eu^{3+} (fibers), and YVO_4:0.05Eu^{3+} (belts), as well as those samples annealed at high temperature, respectively. From the SEM micrograph of Figure 2a, it can be seen that the as-formed YVO_4:0.05Eu^{3+} precursor fibers are uniform with diameters ranging from 100 to 200 nm. In order to obtain pure inorganic fibers, a high-temperature annealing is employed to remove the organic PVP templates. After being calcined at 700 °C for 4 h, the fibers shrink and

(30) (a) Zhou, F.; Zhao, X. M.; Xu, H.; Yuan, C. G. *J. Phys. Chem. C* **2007**, *111*, 1651. (b) Yao, K. X.; Zeng, H. C. *J. Phys. Chem. C* **2007**, *111*, 13301.

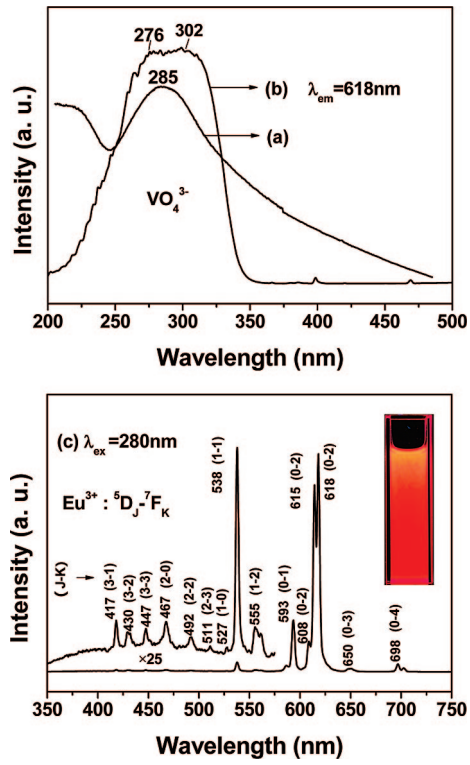

Figure 4. Absorption (a), excitation (b), and emission (c) spectra for YVO_4:0.05Eu^{3+} nanofibers. (The inset shows luminescence photograph of Eu^{3+}-doped YVO_4 nanofibers dispersing in the ethanol solution (0.5 mM).)

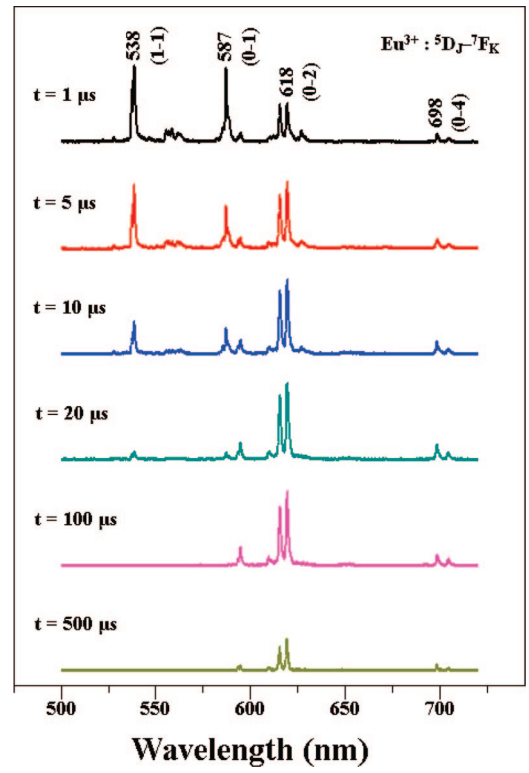

Figure 5. Time-resolved emission spectra of Eu^{3+} in the YVO_4:0.05Eu^{3+} nanofibers (λ_{ex} = 290 nm, laser).

become curvy due to the decomposition of PVP and crystallization of yttrium vanadate. It can also be seen from Figure 2b that the diameters of YVO_4:0.05Eu^{3+} nanofibers become 50−100 nm. By partial replacement of V by P, the as-formed precursor $YP_{0.8}V_{0.2}O_4$:0.05Eu^{3+} samples still present fiberlike morphology and their diameters range from 100 to 200 nm (Figure 2c). Figure 2d shows the SEM image of $YP_{0.8}V_{0.2}O_4$:0.05Eu^{3+} nanofibers obtained after annealing at 700 °C for 4 h, and the fibers (seem to consist of linked particles) have diameters ranging from 50 to 100 nm. The morphology and diameter of electrospun 1D nanomaterials are dependent on a number of processing parameters including the type of polymer, the conformation of polymer chain, electrical conductivity, the surface tension, and the operational conditions. Under controlling these factors, the formation of a skin on the surface of the liquid jet (due to rapid evaporation of solvent) and the subsequent collapse of the skin might be responsible for the emergence of a beltlike morphology.[31] Additionally, a higher flow rate for solution always leads to the formation of thicker fibers, and these thicker fibers without complete drying before reaching the collector may also lead to the formation of beltlike structures with rectangular cross sections.[31b,32] By adjusting some of the electrospun parameters, we can obtain Q-1D hybrid beltlike materials, as shown in Figure 2e. In general, the precursor belts are formed with typical widths of 0.7−2.5 μm and thickness of 300−600 nm. After being annealed at 700 °C for 4 h, the sample keeps the beltlike structure with widths of 0.4−1.5 μm and thickness in the range of 150−300 nm (Figure 2f). The low-magnification SEM images of as-prepared samples are shown in Figure S5 (Supporting Information), which shows that the as-formed 1D or Q-1D samples are uniform with lengths of several tens to hundreds of micrometers before and after annealing at high temperature.

The TEM and HRTEM images of YVO_4:0.05Eu^{3+} and $YP_{0.8}V_{0.2}O_4$:0.05Eu^{3+} nanofibers and YVO_4:0.05Eu^{3+} microbelts are shown in Figure 3. From Figure 3, parts a, c, and e, it can be seen that the nanofibers or microbelts are further composed of fine and closely linked nanoparticles. The typical HRTEM image (Figure 3b) of YVO_4:0.05Eu nanofibers clearly shows lattice fringes with interplanar spacing of 0.36 and 0.27 nm that correspond to the (200) and (112) plane of YVO_4, respectively. Similarly, the lattice fringes [d = 0.36 nm for 200 plane] of $YP_{0.8}V_{0.2}O_4$:0.05Eu^{3+} nanofibers and YVO_4:0.05Eu^{3+} microbelts can also be observed clearly in Figure 3, parts d and f, respectively. These results further confirm the presence of highly crystalline YVO_4:0.05Eu^{3+} and $YP_{0.8}V_{0.2}O_4$:0.05Eu^{3+} in the nanofiber and microbelt samples after annealing at high temperature, agreeing well with the XRD results.

Finally, it should be mentioned that the key strategy of the sol−gel/electrospinning method to obtain 1D inorganic nanomaterials was to form a solution with viscoelastic behavior similar to that of a conventional polymer solution. In our experiments, the purposes of controlling the volume ratio of water to alcohol and the weight percentage of PVP were to adjust the viscoelastic behavior, making the hybrid solution suitable for further electrospinning. Uniform 1D

(31) (a) Krishappa, R. V. N.; Desai, K.; Sung, C. *J. Mater. Sci.* **2003**, *38*, 2357. (b) Li, D.; Xia, Y. N. *Adv. Mater.* **2004**, *16*, 1151. (c) Zhang, Y. F.; Yang, J.; Li, Q.; Cao, X. Q. *J. Cryst. Growth* **2007**, *308*, 180.
(32) Travis, J. S.; Horst, A. V. R. *Biomaterials* **2008**, *29*, 1989.

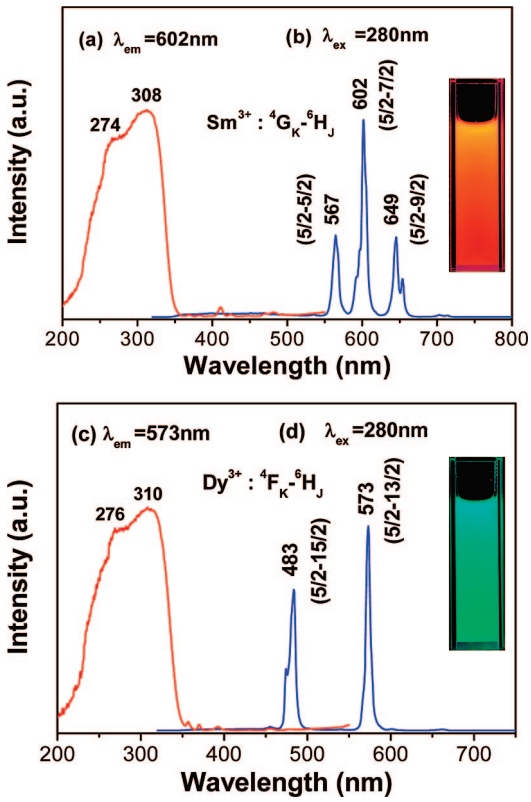

Figure 6. Excitation (a and c) and emission (b and d) spectra for YVO_4:$0.02Sm^{3+}$ (a and b) and YVO_4:$0.02Dy^{3+}$ (c and d) nanofibers. The insets show the corresponding luminescence photographs of the samples dispersed in the ethanol solutions.

morphology cannot be obtained (even no any sample can be obtained) under inappropriate experimental conditions. From the SEM images of YVO_4:$0.05Eu^{3+}$ fiberlike samples obtained by adjusting water/alcohol ratios (a—1:4, b—1:4.25, c—1:4.5, d—1:4.75) (Figure S6, Supporting Information), it can be seen that the yield and morphology of samples vary to some extent. When the water/alcohol ratio reaches or exceeds 1:5, no sample can be obtained by the electrospinning process. The morphology and diameter of electrospun samples are also dependent on a number of process parameters including the intrinsic properties of solution and the operational conditions. In order to obtain uniform 1D morphologies, searching for a balance point of various electrospinning parameters is very important. In our experiments, the balance point might be related to the volume ratio of water to alcohol, the weight percentage of PVP, the spinning rate, the strength of electric field, and the distance between the spinneret and collector. The synthesis conditions listed in Supporting Information Table S1 are the optimized ones for the corresponding morphologies.

3.2. Luminescence Properties. *3.2.1. Photoluminescence Properties.* Under short wavelength UV irradiation, YVO_4:Ln nanofibers exhibit red, orange-red, and green emission for Ln = Eu^{3+}, Sm^{3+}, and Dy^{3+}, respectively. Figure 4a shows the UV—vis absorption spectrum of YVO_4:$0.05Eu^{3+}$ nanofibers dispersed in ethylene glycol. A strong absorption band peaking at 285 nm is observed, agreeing well with the reported absorption spectra of colloid solution of nanocrystalline YVO_4:Eu^{3+}.[23b,33] Obviously, this band is attributed to a charge transfer from the oxygen ligands to the central vanadium atom within the VO_4^{3-} group ions. From the viewpoint of molecular orbital theory, it corresponds to transitions from the $^1A_2$ ($^1T_1$) ground state to $^1A_1$ (^1E) and ^1E ($^1T_2$) excited states of VO_4^{3-} ions. Figure 4 shows excitation (b) and emission (c) spectra for YVO_4:$0.05Eu^{3+}$ nanofibers annealed at 700 °C in the UV—vis spectral region, respectively. The excitation spectrum was obtained by monitoring the emission of Eu^{3+} $^5D_0$—$^7F_2$ transition at 618 nm. It can be seen clearly that the excitation spectrum consists of a broad intense band from 200 to 350 nm due to VO_4^{3-} ions, fitting well with the absorption spectrum (Figure 4a). This confirms that the emission of Eu^{3+} occurs via an energy transfers from the excited VO_4^{3-}. The mechanism of this energy transfer is well-known as the subject of some investigations.[34] Excitation into the VO_4^{3-} group at 280 nm yields the emission spectrum corresponding the f—f transitions of Eu^{3+}, which is dominated by the red emission $^5D_0$—$^7F_2$ transition at 618 nm (Figure 4c). The strong red light emission of the nanofiber solution upon excitation at 254 nm with a UV lamp can be seen clearly (inset of Figure 4c). The emission spectrum not only contains the characteristic transition lines from the lowest excited $^5D_0$ level of Eu^{3+} but also those from higher energy levels ($^5D_1$, $^5D_2$, $^5D_3$) of Eu^{3+} with a very weak intensity (which can be seen more clearly by enlarging the emission spectrum in the short wavelength region). No emission from the VO_4^{3-} group is observed with the excitation of 280 nm UV, suggesting that the energy transfer from VO_4^{3-} to Eu^{3+} is quite efficient. In addition, the crystal field splitting of Eu^{3+} $^5D_0$—$^7F_{1,2,4}$ transitions can be seen clearly, indicating that the YVO_4:$0.05Eu^{3+}$ nanofibers are well crystallized (agreeing well with the XRD and HRTEM results). The emission spectrum of YVO_4:$0.05Eu^{3+}$ nanofibers agrees well with other types of YVO_4:Eu^{3+} materials reported previously.[20b,23b,24d] The whole excitation and emission process of YVO_4:Eu^{3+} under UV radiation include three major steps. The first is absorption of UV radiation by VO_4^{3-} groups, then the excited energy is subsequently transferred to Eu^{3+} ions after a thermally activated energy migration through the vanadate sublattice, and the final one is the deexcitation process of excited Eu^{3+} ions, producing strong red emissions. The excitation and emission process of VO_4^{3-}, energy transfer process from VO_4^{3-} to Eu^{3+}, as well as the emission process of Eu^{3+} are schematically shown in Figure S7 (Supporting Information).

In order to obtain more information about the kinetic properties for the luminescence of Eu^{3+} in YVO_4:$0.05Eu^{3+}$ nanofibers, time-resolved emission spectra of YVO_4:$0.05Eu^{3+}$ nanofibers were measured at room temperature by excitation into the VO_4^{3-} band with a 290 nm laser. By analyzing the time-resolved emission spectra, the relaxation process from $^5D_1$ to $^5D_0$ for the luminescence of Eu^{3+} can be better understood. The emission spectra collected at different delay times (t) ranging from 1 to 500 μs are shown

(33) (a) Huignard, A.; Gacoin, T.; Boilot, J. P. *Chem. Mater.* **2000**, *12*, 1090. (b) Yan, C. H.; Sun, L. D.; Liao, C. S. *Appl. Phys. Lett.* **2003**, *82*, 3511.
(34) (a) Huignard, A.; Buissette, V.; Franville, A. C.; Gacoin, T.; Boilot, J. P. *J. Phys. Chem. B* **2003**, *107*, 6754. (b) Blasse, G.; Bril, A. *Philips Tech. Rev.* **1970**, *31* (10), 304.

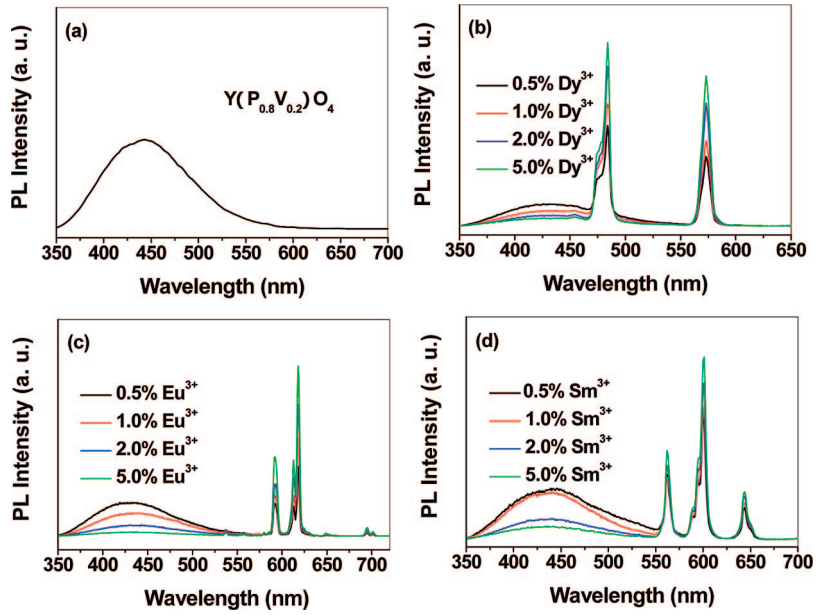

Figure 7. Emission spectra (λ_{ex} = 280 nm) for (a) $YP_{0.8}V_{0.2}O_4$ nanofibers, (b) $Y_{1-x}P_{0.8}V_{0.2}O_4$:xDy^{3+} nanofibers (x = 0.005, 0.01, 0.02, and 0.05), (c) $Y_{1-x}P_{0.8}V_{0.2}O_4$:xEu^{3+} nanofibers (x = 0.005, 0.01, 0.02, and 0.05), and (d) $Y_{1-x}P_{0.8}V_{0.2}O_4$:xSm^{3+} nanofibers (x = 0.005, 0.01, 0.02, and 0.05).

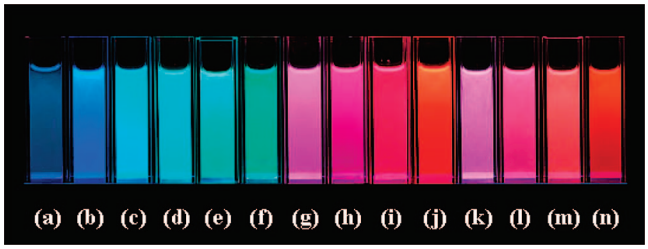

Figure 8. Luminescence photographs of YVO_4 and $Y_{1-x}P_{0.8}V_{0.2}O_4$:xLn nanofibers dispersed in the ethanol solutions: (a) YVO_4; (b) $Y(P_{0.8}V_{0.2})O_4$; (c−f) $Y_{1-x}P_{0.8}V_{0.2}O_4$:xDy^{3+} (x = 0.005, 0.01, 0.02, and 0.05); (g−j) $Y_{1-x}P_{0.8}V_{0.2}O_4$:xEu^{3+} (x = 0.005, 0.01, 0.02, and 0.05); (k−n) $Y_{1-x}P_{0.8}V_{0.2}O_4$:xSm^{3+} (x = 0.005, 0.01, 0.02, and 0.05).

in Figure 5. Under the excitation of 290 nm laser, an electron is excited from the ground state to the excited state of VO_4^{3-}, from which the electron rapidly relaxes to higher excited Eu^{3+} ^{5}D states (^{5}D$_{1,2,3}$) first, then to lowest ^{5}D$_0$ excited state, and emissions are produced by radiative transitions from the excited ^{5}D states (mainly ^{5}D$_0$) to the ground ^{7}F$_J$ (J = 0−4) states, as schematically shown in Supporting Information Figure S7. It can be seen that as the delay time increased from 1 to 20 μs, the intensity of the emissions from ^{5}D$_1$−^{7}F$_1$ (538 nm) and ^{5}D$_0$−^{7}F$_1$ (587 nm) decreased dramatically. Meanwhile, ^{5}D$_0$ excited states can be observed clearly and the emission of ^{5}D$_0$−^{7}F$_2$ (618 nm) and ^{5}D$_0$−^{7}F$_4$ (698 nm) begins to increase. This is indicative of an electron relaxation process from the ^{5}D$_1$ to ^{5}D$_0$ state. When t = 100 μs, the ^{5}D$_1$−^{7}F$_1$ emission becomes undetectable with respect to the ^{5}D$_0$−^{7}F$_2$ emission. When t > 500 μs, the ^{5}D$_0$−^{7}F$_2$ emission also begins to decay gradually due to the depopulation of the excited states (figures are not shown due to the limited space).

In order to study the decay behaviors of Eu^{3+} luminescence in more detail in the YVO_4:0.05Eu^{3+} nanofibers and microbelts, the kinetic decay curves for the representative emission of Eu^{3+} ^{5}D$_1$−^{7}F$_1$ (538 nm) and ^{5}D$_0$−^{7}F$_2$ (618 nm, main emission) were measured, as shown in Figure S8 (Supporting Information). All the decay curves can be well fitted into single-exponential function as $I = I_0 \exp(-t/\tau)$, and the lifetime τ values can be determined.[19c,e] The fluorescence lifetimes for the ^{5}D$_1$ state (measured for ^{5}D$_1$−^{7}F$_1$ at 538 nm) are 7.35 μs in YVO_4:0.05Eu^{3+} microbelts (Supporting Information Figure S8a) and 7.66 μs in YVO_4:0.05Eu^{3+} nanofibers (Supporting Information Figure S8b), while those of the ^{5}D$_0$ state (measured for ^{5}D$_0$−^{7}F$_2$ at 618 nm) are 0.45 ms in microbelts (Supporting Information Figure S8c) and 0.52 ms in nanofibers (Supporting Information Figure S8d), respectively, basically agreeing with the results for Eu^{3+} in other nanostructured YVO_4 materials.[24e,35]

The room-temperature excitation and emission spectra of the other rare earth ions Sm^{3+}- and Dy^{3+}-doped YVO_4 nanofibers are given in Figure 6. The excitation spectra for YVO_4:0.02Sm^{3+} and YVO_4:0.02Dy^{3+} nanofibers are very similar to those in Figure 4b; that is, monitored with 605 nm emission of Sm^{3+} (^{4}G$_{5/2}$−^{6}H$_{7/2}$) or 573 nm emission of Dy^{3+} (^{4}F$_{9/2}$−^{6}H$_{13/2}$), a strong and broad band due to the VO_4^{3-} group has been observed. Excitation into the vanadate group at 280 nm yields the characteristic red-orange emission of Sm^{3+} at 567 nm (^{4}G$_{5/2}$−^{6}H$_{5/2}$, green), 602 nm (^{4}G$_{5/2}$−^{6}H$_{7/2}$, orange), and 649 nm (^{4}G$_{5/2}$−^{6}H$_{9/2}$, red) and blue-yellow emission of Dy^{3+} at 483 nm (^{4}F$_{9/2}$−^{6}H$_{15/2}$, blue) and 573 nm (^{4}F$_{9/2}$−^{6}H$_{13/2}$, yellow), respectively. This indicates that the same situation is holding for Sm^{3+}- and Dy^{3+}-doped YVO_4 nanofibers, i.e., an efficient energy transfer also occurs from VO_4^{3-} to Sm^{3+} and Dy^{3+}. Upon excitation at 254 nm with a UV lamp, corresponding luminescence photographs of the YVO_4:0.02Sm^{3+} and YVO_4:0.02Dy^{3+} nanofibers dispersed in the ethanol solutions (0.5 mM) are shown in the insets of Figure 6. The PL decay curves for the luminescence of Sm^{3+} (^{4}G$_{5/2}$−^{6}H$_{7/2}$) and Dy^{3+} (^{4}F$_{9/2}$−^{6}H$_{13/2}$) in microbelts and nanofibers were measured at room temper-

(35) Kang, W. Y.; Park, J. S.; Kim, D. K.; Suh, K. S. *Bull. Korean Chem. Soc.* **2001**, *22*, 921.

ature, as shown in Figure S9 (Supporting Information). All the decay curves can be well fitted into single-exponential function as $I = I_0 \exp(-t/\tau)$. The fluorescence lifetimes for $^4G_{5/2}$ (detected at 602 nm) of Sm^{3+} were determined to be 0.46 ms in microbelts and 0.5 ms in nanofibers, and those of $^4F_{9/2}$ (detected at 573 nm) of Dy^{3+} were determined to be 0.13 ms in microbelts and 0.15 ms in nanofibers, respectively.

In comparison with vanadate phosphors, the phosphate−vanadate phosphors are more stable and have better luminescent properties at high temperature.[36] Riwotzki and Haase investigated the luminescence and energy transfer processes in $YP_{0.95}V_{0.05}O_4$:Eu nanoparticles in detail.[24e] Additionally, with phosphate groups (PO_4^{3-}) doping into the YVO_4:Ln nanocystals, the color of the emission can be easily modulated by single-wavelength excitation.[25b] The $YP_{0.8}V_{0.2}O_4$ nanofibers exhibit a broad emission centered at approximately 440 nm (Figure 7a) with a bright blue color upon excitation at 254 nm with a UV lamp (Figure 8b), whereas the pure YVO_4 nanofibers dispersed in the ethanol solutions (0.5 mM) exhibit weak blue emission under excitation at 254 nm with a UV lamp (Figure 8a). The introduction of phosphorus (PO_4^{3-}) into the YVO_4 lattice would increase the V−V separation and hamper the efficient energy transfer from VO_4^{3-} groups to the quenching sites, resulting in more strong emission from the VO_4^{3-} groups. The luminescent properties change greatly when the VO_4^{3-} is partly replaced by PO_4^{3-} in the fibers, as shown in Figure 7 for $Y_{1-x}P_{0.8}V_{0.2}O_4$:xLn nanofiber samples. The emission spectra consist of two parts, a broad band from 350 to 550 nm with a maximum around 430 nm (blue emission from the VO_4^{3-} group) and some narrow bands from 570 to 720 nm (Eu^{3+}, red emission), 550 to 700 nm (Sm^{3+}, orange-red emission), and 480 to 650 nm (Dy^{3+}, green emission). Obviously, the former is due to the emission from the VO_4^{3-} group, and the latter is due to $^5D_0-{}^7F_J$ ($J = 1, 2, 3, 4$) emission lines of Eu^{3+}, $^4G_{2/5}-{}^6H_J$ ($J = {}^5/_2, {}^7/_2, {}^9/_2$) emission lines of Sm^{3+}, and $^4F_{9/2}-{}^6H_J$ ($J = {}^{11}/_2, {}^{13}/_2, {}^{15}/_2$) emission lines of Dy^{3+}, respectively. By varying the concentrations of the Ln dopants, the relative emission intensity of VO_4^{3-} to Ln ions can be manipulated with high precision. As shown in Figure 7, $YP_{0.8}V_{0.2}O_4$ nanofibers doped with increasing concentrations of Eu^{3+}, Dy^{3+}, and Sm^{3+} ions (0.5−5 mol%) exhibit decreasing emission intensity ratios of VO_4^{3-} to the Ln dopants. With the increase of Ln ions concentration, energy transfer from the VO_4^{3-} groups to the Ln dopants becomes efficient. Figure 8 shows luminescence photographs of $Y_{1-x}P_{0.8}V_{0.2}O_4$:xLn nanofibers ethanol solutions (0.5 mM) upon excitation with 254 nm from a UV lamp, in which tuning of the emission color from blue to green (Figure 10c−f, $Y_{1-x}P_{0.8}V_{0.2}O_4$:$x$$Dy^{3+}$), red (Figure 10g−j, $Y_{1-x}P_{0.8}V_{0.2}O_4$:$x$$Eu^{3+}$), and orange-red (Figure 10k−n, $Y_{1-x}P_{0.8}V_{0.2}O_4$:$x$$Sm^{3+}$) can be realized.

3.2.2. Cathodoluminescence Properties. Under low-voltage electron beam excitation, the as-prepared YVO_4:Ln (Eu^{3+}, Sm^{3+}, Dy^{3+}) microbelts and nanofibers also exhibit the same red, orange-red, and green emissions as the UV excitation, respectively. The representative CL spectra of the YVO_4:Ln microbelts and nanofibers under the excitation of electron beam (accelerating voltage = 3 kV; filament current = 15 mA) are shown in Figure 9, which have identical shapes as the PL emission spectra. From the typical CL spectra, it can be seen that the microbelt phosphors have a higher CL intensity than that of nanofibers phosphors (all the experimental conditions were kept identical in order to avoid experimental errors.) Defects have serious drawback in luminescence intensity for phosphors as they provide nonradiative recombination routes for electrons and holes.[37] From the HRTEM images shown in Figure 3, it is clear that YVO_4:Eu^{3+} nanofibers have a number of defect regions (Figure 3b) and no obvious defects are found within the

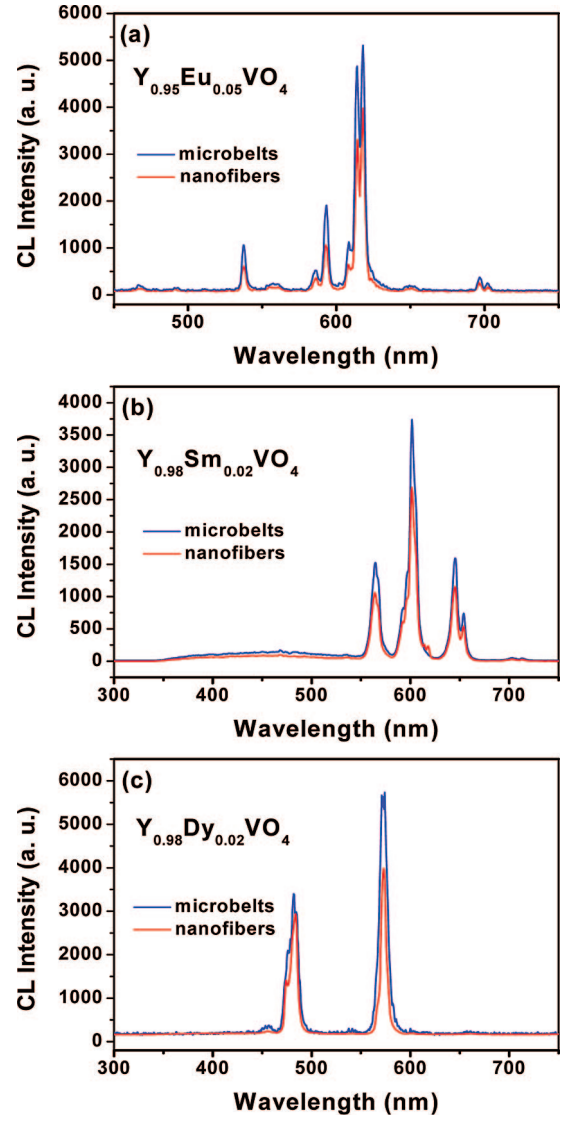

Figure 9. Typical cathodoluminescence spectra of YVO_4:Ln (Ln = Eu^{3+}, Sm^{3+}, Dy^{3+}) microbelts and nanofibers: (a) YVO_4:0.05Eu^{3+}; (b) YVO_4:0.02Sm^{3+}; (c) YVO_4:0.02Dy^{3+}. (Accelerating voltage, 3 kV; filament current, 15 mA.)

(36) Blasse, G.; Grabmaier, B. C. *Luminescent Materials*; Springer: Berlin, 1994.

(37) (a) Wan, J. X.; Wang, Z. H.; Chen, X. Y.; Mu, L.; Qian, Y. T. *J. Cryst. Growth* **2005**, *284*, 538. (b) Yang, J.; Liu, X. M.; Li, C. X.; Quan, Z. W.; Kong, D. Y.; Lin, J. *J. Cryst. Growth* **2007**, *303*, 480. (c) Yang, J.; Li, C. X.; Cheng, Z. Y.; Zhang, X. M.; Quan, Z. W.; Zhang, C. M.; Lin, J. *J. Phys. Chem. C* **2007**, *111*, 18148–18154.

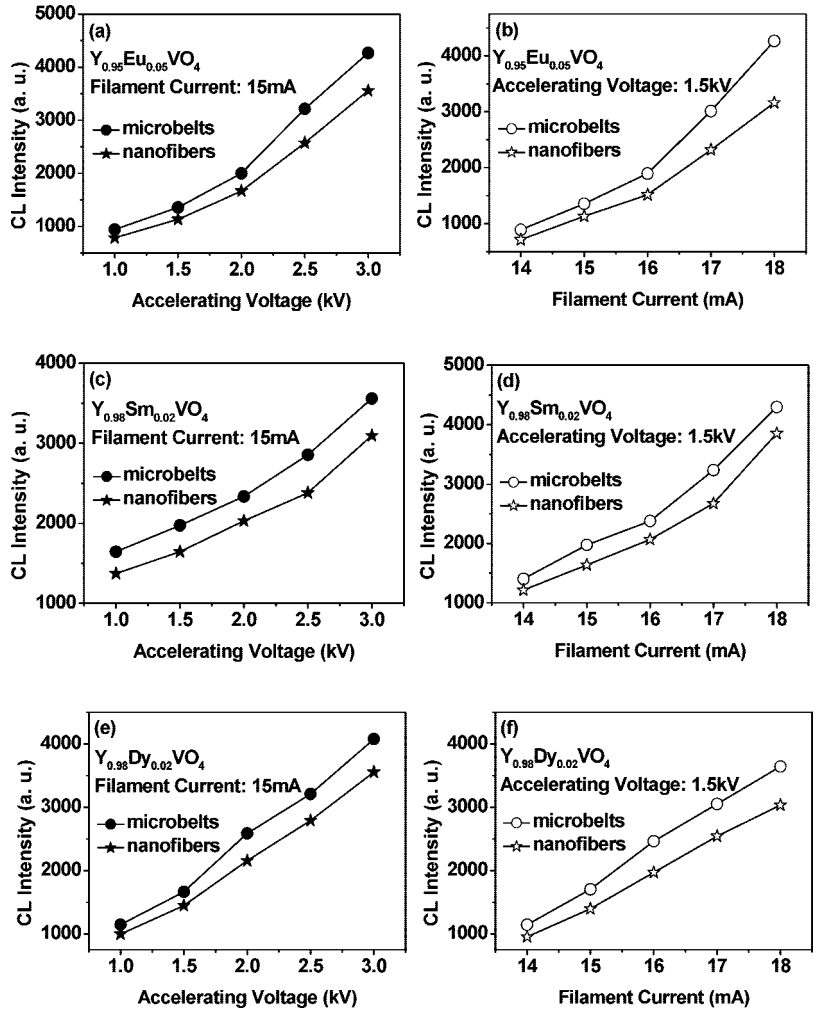

Figure 10. Cathodoluminescence intensity of YVO_4:Ln (Ln = Eu^{3+}, Sm^{3+}, Dy^{3+}) microbelts and nanofibers as a function of accelerating voltage (a, c, e) and filament current (b, d, f).

crystal structure of YVO_4:Eu^{3+} microbelts (Figure 3f). The large surface area introduces a large number of defects into the phosphor crystal. Herein, the surface areas of the as-prepared YVO_4:Ln microbelts are much smaller than those of YVO_4:Ln nanofibers. This is the reason that the CL intensity of microbelts is higher than that of nanofibers. The CL emission intensities for the YVO_4:Ln microbelts and nanofiber phosphors have been investigated as a function of the filament current and the accelerating voltage, as shown in Figure 10, respectively. The CL intensity increased with the accelerating voltage from 1 to 3 kV (Figure 10, parts a, c, and e). Similarly, when the accelerating voltage is fixed at 1.5 kV, the CL intensity also increases with raising the filament current from 14 to 18 mA (Figure 10, parts b, d, and f). The increase in CL brightness with an increasing electron energy and filament current can be attributed to deeper penetration of electrons into the phosphors and the larger electron beam current density. The electron penetration depth can be estimated using the empirical formula $L[\text{Å}] = 250(A/\rho)(E/Z^{1/2})^n$, where $n = 1.2/(1 - 0.29 \log_{10} Z)$, A is the atomic or molecular weight of the material, ρ is the bulk density, Z is the atomic number or the number of electrons per molecule in the case compounds, and E is the accelerating voltage (kV).[38] For CL, the Eu^{3+}, Sm^{3+}, Dy^{3+} ions are excited by the plasma produced by the incident electrons. The deeper the electron penetration depth, the more the plasmons will be produced, which resulted in more Eu^{3+}, Sm^{3+}, Dy^{3+} ions being excited and thus the CL intensity increased.

4. Conclusions

In summary, YVO_4:Ln and $YP_{0.8}V_{0.2}O_4$:Ln (Ln = Eu^{3+}, Sm^{3+}, Dy^{3+}) 1D nanofibers and YVO_4:Ln Q-1D microbelts have been successfully synthesized by means of the electrospinning technique in conjunction with the sol−gel process. Due to an efficient energy transfer from the VO_4^{3-} group to the lanthanide ions (Ln), the Eu^{3+}, Sm^{3+}, and Dy^{3+} show their characteristic strong emissions in the YVO_4 nanofibers upon excitation into the VO_4^{3-} group at 280 nm. Under low-voltage electron beam excitation, microbelt phosphors have a higher CL intensity than the nanofiber phosphors due to lower defect concentration in the former. In addition, with PO_4^{3-} ions partial replacement of the VO_4^{3-} ions, multicolor tuning emissions of the $YP_{0.8}V_{0.2}O_4$:Ln nanofibers can be achieved. These studies indicate a facile route for the development 1D and Q-1D luminescent nanomaterials that are useful in many types of color display fields.

(38) Feldman, C. *Phys. Rev.* **1960**, *117*, 455.

Acknowledgment. This project is financially supported by the foundation of "Bairen Jihua" of the Chinese Academy of Sciences, National Basic Research Program of China (2003CB-314707, 2007CB935502), and the National Natural Science Foundation of China (NSFC 50572103, 50872131, 20431030, 00610227).

Supporting Information Available: Detailed experimental conditions and the corresponding morphologies (Table S1), nominal and analyzed compositions (Table S2), XRD patterns for YVO_4:0.05Eu^{3+} microbelts and $Y(P_{0.8}V_{0.2})O_4$:0.05Eu^{3+} nanofibers (Figure S1), XRD patterns for YVO_4:Ln nanofibers (Figure S2), FT-IR spectra of YVO_4:0.05Eu^{3+} nanofibers (Figure S3), TG−DTA curves of as-formed precursor for YVO_4:0.05Eu^{3+} fibers (Figure S4), low-magnification SEM images of the samples (Figure S5), SEM images for YVO_4:0.05Eu^{3+} nanofibers obtained by adjusting water/alcohol ratio (Figure S6), the scheme for VO_4^{3-}−Eu^{3+} energy transfer and Eu^{3+} emission process (Figure S7), the decay curves for Eu^{3+} in YVO_4:0.05Eu^{3+} microbelts and nanofibers (Figure S8), and the decay curves for Sm^{3+} in YVO_4:0.02Sm^{3+} samples and Dy^{3+} in YVO_4:0.02Dy^{3+} samples (Figure S9). This material is available free of charge via the Internet at http://pubs.acs.org.

CM801538T